RSC Advances

PAPER

View Article Online
View Journal | View Issue

Cite this: *RSC Adv.*, 2025, **15**, 35543

Silver chloride–poly-2-chlorobenzeneamine complex nanocomposite as photoelectrode for photoelectrochemical hydrogen gas generation from seawater

Fahad Abdulaziz,[a] Mohamed Rabia,[b] Mohamed Zayed,*[c] Salman Latif,[a] Yassin A. Jeilani,[a] Raja Rama Devi Patel,[d] Hussein A. Elsayed[e] and Ashour M. Ahmed[f]

An innovative silver chloride–poly(2-chlorobenzeneamine) (AgCl–P2CBA) complex nanocomposite is developed through a one-step chemical synthesis route for efficient and sustainable hydrogen production from seawater. The resulting nanocomposite exhibits a rough, heterogeneous surface morphology, an optical bandgap of 1.92 eV, and an average crystallite size of approximately 40 nm, which collectively enhance its light-harvesting and photoresponse properties. The integration of AgCl into the polymeric matrix not only improves visible-light absorption but also facilitates more effective charge carrier separation, leading to a marked increase in photocurrent density from −0.011 mA cm^{-2} (pure P2CBA) to −0.035 mA cm^{-2} for the composite. Under solar illumination, the AgCl–P2CBA photocathode achieved a hydrogen evolution rate of 3.5 μmol h^{-1} cm^{-2} using untreated seawater, demonstrating excellent activity and stability. Additionally, the electrode remained responsive across a broad photon energy range (1.7–3.6 eV), underscoring its adaptability to diverse lighting conditions. This work presents an innovative combination of a halide salt with a chlorinated conducting polymer, offering a simple, scalable, and cost-effective photoelectrode design with strong potential for practical hydrogen generation technologies.

Received 12th May 2025
Accepted 11th September 2025

DOI: 10.1039/d5ra03341a

rsc.li/rsc-advances

1. Introduction

Hydrogen is widely regarded as a clean, renewable, and sustainable energy alternative. Recently, photoelectrochemical (PEC) water splitting has gained recognition as a promising technology for hydrogen production.[1,2] Seawater offers several advantages for PEC hydrogen production, including being an abundant and renewable resource, a low-cost feedstock, and highly feasible for large-scale hydrogen production. Additionally, seawater naturally contains dissolved ions and trace metals, which enhance the electrolyte's conductivity and facilitate charge transfer during the PEC process. In PEC systems, water is split into hydrogen and oxygen under light illumination in the presence of semiconductors.[3] These semiconductors function as light absorbers, converting light energy into free electrons and holes with sufficient thermodynamic potential to drive the water-splitting reaction.[4,5] The development of efficient semiconductor photocatalysts is vital for achieving high performance and cost-effectiveness in PEC applications. The photochemistry of silver halides has long been established, with applications spanning various industries. Among them, silver chloride (AgCl) has garnered significant interest for photocatalysis in water splitting due to its high photosensitivity. AgCl's photoactivity extends from the UV to the visible light spectrum, primarily driven by self-sensitization.[6,7] Furthermore, AgCl exhibits potential as a p-type semiconductor. It has large bandgap energy significantly influenced by impurities and Frenkel defects in its crystal structure.[8] Beyond photocatalysis, AgCl finds applications in antimicrobials, disinfectants, photography, photochromic lenses for sunglasses, and infrared-transmissive optical components for windows. The PEC of AgCl is low due to limited charge transfer efficiency and high energy gap.

Polymer materials have also drawn considerable attention for PEC electrode applications.[9,10] This is thanks to their

[a]*Department of Chemistry, College of Science, University of Ha'il, Ha'il, 81451, Saudi Arabia*

[b]*Nanomaterials Science Research Laboratory, Chemistry Department, Faculty of Science, Beni-Suef University, Beni-Suef, Egypt*

[c]*Nanophotonics and Applications Lab (NPA), Physics Department, Faculty of Science, Beni-Suef University, Beni-Suef 62514, Egypt. E-mail: m.zayed88ph@yahoo.com*

[d]*Department of Biology, College of Science, University of Ha'il, Ha'il 55473, Saudi Arabia*

[e]*Department of Physics, College of Science, University of Ha'il, P. O. Box 2440, Ha'il, Saudi Arabia*

[f]*Physics Department, College of Science, Imam Mohammad Ibn Saud Islamic University (IMSIU), Riyadh, 11623, Saudi Arabia*

properties such as light-harvesting capability, tunable electronic structures, high surface area, and abundant active sites.[11] Additionally, polymers are lightweight, eco-friendly, flexible, low-cost, and easy to fabricate into large-area devices.[10,12] Poly(2-chlorobenzeneamine) (P2CBA) is a polymer with a unique conjugated structure that makes it highly suitable for various optical applications. The presence of a conjugated system allows this polymer to interact effectively with optical photons, enabling it to absorb light energy efficiently. This absorption process results in the excitation of electrons, leading to the liberation of high-energy (hot) electrons. These hot electrons can then transfer through an external medium, facilitating critical redox reactions, such as the reduction of water molecules. This process ultimately leads to the generation of hydrogen gas, which is an essential component for renewable energy applications.

Furthermore, the efficiency of P2CBA in optical applications can be significantly enhanced by combining it with other materials that contribute additional optical properties. The integration of nanomaterials, metal oxides, or other conjugated systems can improve its absorption range, charge separation efficiency, and overall photophysical behavior. This synergistic effect results in a more effective photochemical system, optimizing hydrogen production through photocatalysis. The ability of P2CBA to be modified and tuned for specific applications makes it a promising candidate for sustainable energy solutions. Its flexible properties and compatibility with other advanced materials make it an exciting area of research in the field of optoelectronics and green energy technology. One of the major limitations in previous studies is the reliance on freshwater as the hydrogen source, often requiring the addition of strong acids, bases, or specialized electrolytes like ammonia to facilitate the reaction. This approach poses challenges in terms of sustainability, cost, and scalability. Therefore, the use of readily available, commercially viable electrolytes-such as seawater-represents a crucial step forward in developing practical and sustainable hydrogen production systems for future energy technologies.

In this study, a novel AgCl–P2CBA nanocomposite is developed by integrating the distinctive optoelectronic properties of P2CBA with the excellent photonic activity of AgCl through a simple, one-step synthesis process. The combination leverages the semiconducting nature of P2CBA-characterized by its strong visible-light absorption and enhanced electrical conductivity-alongside AgCl's high electron mobility and superior light-induced charge generation. The chlorinated aromatic structure and amine groups of P2CBA promote effective interfacial interactions with AgCl, resulting in improved structural integration, facilitated charge transfer, and enhanced surface functionalization. Uniquely, the polymer serves not only as an active light-absorbing material but also as a structural binder that maintains the stability and integrity of the composite during operation. This hybrid design leads to significantly enhanced light-harvesting efficiency, more effective charge separation, and improved photoelectrochemical (PEC) stability under saline conditions. For the first time, this study introduces the AgCl–P2CBA nanocomposite as a visible-light-driven photocathode for direct hydrogen generation from seawater, addressing the challenges of cost, durability, and performance. Comprehensive characterization-including structural, morphological, and optical analyses-is performed, alongside detailed PEC evaluations under dark, white light, and monochromatic conditions. The photocurrent response, chopping current behavior, and hydrogen evolution rate collectively validate the potential of this nanocomposite as a cost-effective, scalable, and high-efficiency material for green hydrogen production on an industrial scale.

2. Materials & methods

2.1. Materials

In this study, various high-purity materials were utilized. Silver nitrate ($AgNO_3$, 99.9%), 2-chlorobenzenamine (99.9%), and acetic acid (CH_3COOH, 99.8%) were sourced from Merck, Germany. Hydrochloric acid (HCl, 36%) and ammonium persulfate ($(NH_4)_2S_2O_8$, 99.8%) were obtained from Pio-Chem Co., Egypt. Additionally, seawater was collected from the Red Sea for the PEC experiments.

2.2. Synthesis of P2CBA and AgCl–P2CBA

The AgCl–P2CBA complex nanocomposite was synthesized through the deposition of silver chloride (AgCl) onto the surface of 2-chlorobenzenamine, facilitated by the reaction between silver ions (Ag^+) and chloride ions (Cl^-). This process occurred concurrently with the polymerization of 2-chlorobenzenamine, resulting in the formation of a composite material. To initiate the reaction, 2-chlorobenzenamine (0.06 M) was dissolved in acetic acid (1.0 M). Subsequently, ammonium persulfate (0.07 M) and silver nitrate (0.07 M) were added to the solution. This mixture led to the formation of the AgCl–P2CBA complex as a thin film deposited on a glass substrate. The reaction mixture was allowed to proceed under continuous stirring at room temperature for two days to ensure homogeneity and completeness of the polymerization and deposition processes.

An alternative method for the synthesis involved the formation of pristine P2CBA. In this process, 2-chlorobenzenamine was polymerized without the presence of silver ions. Here, a higher concentration of ammonium persulfate (0.14 M) was used as the oxidizing agent, while the monomer was dissolved in hydrochloric acid (HCl) instead of acetic acid. This variation resulted in the formation of pure P2CBA, highlighting the influence of reaction conditions on the final product. Both methods emphasized the critical role of oxidant concentration and reaction medium in determining the composite structure and properties.

2.3 Characterization techniques

The physico-chemical properties of P2CBA and AgCl–P2CBA materials were analyzed using various characterization techniques. X-ray diffraction (XRD; Bruker D8-Advance) was used to determine the crystal structure and phase of the P2CBA and AgCl–P2CBA materials. The surface morphology was characterized by scanning electron microscopy (SEM; Zeiss Sigma 500

VP). The optical properties of the prepared materials were studied using a UV-Vis spectrophotometer (PerkinElmer Lambda) to investigate light absorption and bandgap energy. Fourier transform infrared spectroscopy (FTIR; Bruker) was employed to analyze the functional groups attached to the prepared materials. The oxidation states and chemical surface compositions were examined by X-ray photoelectron spectroscopy (XPS; Shimadzu).

2.4. Photoelectrochemical (PEC) measurement

The photoelectrochemical performance was evaluated using a three-electrode workstation (CHI) for hydrogen generation. Natural Red Sea water was used as the electrolyte. P2CBA and AgCl–P2CBA with an area of 1.0×1.0 cm^2 were employed as the working electrodes. Calomel electrode served as the reference electrode, and a graphic rode was used as the counter electrode. Linear sweep voltammetry (LSV) was conducted to measure the photocurrent density under various reaction conditions, including exposure to white light (400 W metal halide lamp) and in the absence of light (dark conditions). The electrodes' responses to different wavelengths of light were also evaluated.

3. Results and discussion

3.1. Physico-chemical characterization

3.1.1. XRD, FTIR, and XPS analyses. FTIR spectroscopy results for the synthesized P2CBA and AgCl–P2CBA are shown in Fig. 1(a). Table 1 summarizes the functional groups present in the pristine P2CBA polymer and AgCl–P2CBA composite. Specifically, the AgCl–P2CBA composite exhibits absorption bonds at 1620 cm^{-1}, 1580 cm^{-1}, and 1504 cm^{-1}, compared to the corresponding peaks at 1570 cm^{-1} and 1492 cm^{-1} in the pristine P2CBA polymer. These shifts indicate modifications in the aromatic ring structure resulting from AgCl integration. Additionally, the evaluation highlights the substitution effect of the chloride atom within the ring structure. The AgCl–P2CBA composite shows a bond at 825 cm^{-1}, compared to 819 cm^{-1} in the pristine polymer, which confirms the successful insertion of AgCl through complex formation. The shifts in bond positions of vibrational modes across various functional groups confirm the integration of AgCl into the P2CBA polymer matrix. The strong interactions between AgCl and P2CBA lead to alterations in bonding environments and molecular arrangements, which ultimately affect the material's properties. This results in changes to the structural, electronic, and optical characteristics of the composite.

Table 1 Present the band position of functional groups of the AgCl–P2CBA complex composite and the P2CBA pure polymer

Bonds position (cm^{-1})		
P2CBA	AgCl–P2CBA	Groups
3230	3141	N–H
1570, 1492	1620, 1580, 1504	P2CBA ring[13,14]
1402	1400	C–N[15]
1279, 1196	1295, 1199	C–H[16]
819	825	Disubstituted
1090	1050	C–H bending

XPS analysis is conducted to examine the elemental composition and oxidation states within the AgCl–P2CBA complex nanocomposite, as displayed in Fig. 1(b) and (c). The structural integrity of the polymer is evaluated by analyzing the transitions

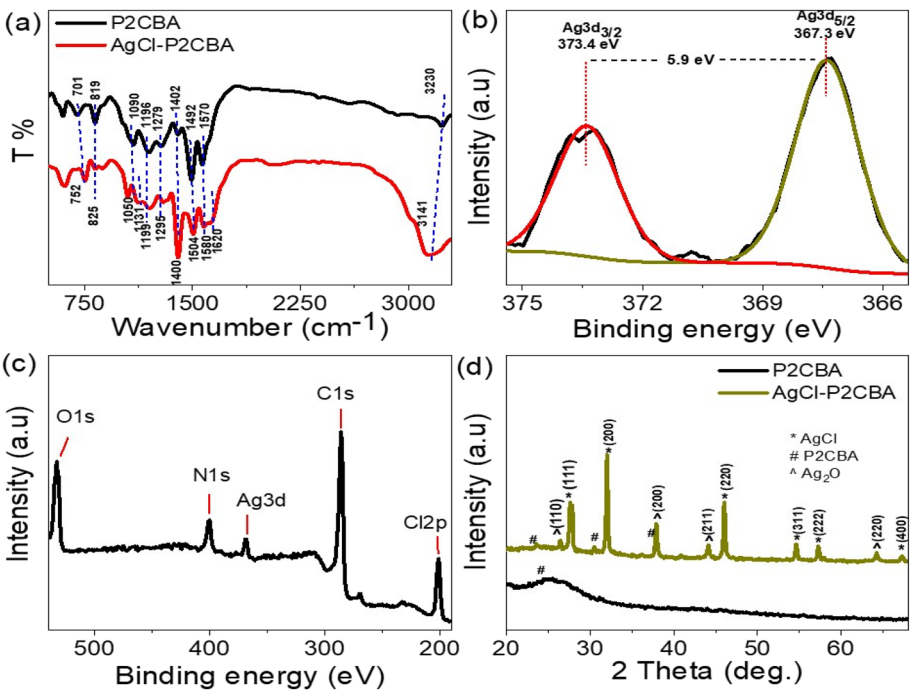

Fig. 1 (a) FTIR spectrum, (b and c) XPS, and (d) XRD patterns analyses of the synthesized pure P2CBA polymer and AgCl–P2CBA complex nanocomposite.

associated with the organic elements in the complex. Characteristic binding energies for carbon (C), nitrogen (N), and chlorine (Cl) were observed at 285.6 eV (C 1s), 400 eV (N 1s), and 201 eV (Cl 2p), respectively, as shown in Fig. 1(c). These transitions provide valuable insights into the chemical environment and bonding characteristics within the polymer framework.

The presence of silver (Ag) (Fig. 1(b)) is confirmed through distinct transitions of Ag $3d_{5/2}$ and Ag $3d_{3/2}$, located at binding energies of 367.3 eV and 373.4 eV, respectively. These peaks confirm the formation of silver in the form of AgCl, embedded within the polymer matrix. Silver is a core component of the AgCl–P2CBA composite. This detailed characterization reflects the unique composition of the nanocomposite, emphasizing its potential for various applications.

The crystallite size and growth orientation of poly(2-chlorobenzeneamine) (P2CBA) and its composite with silver chloride (AgCl–P2CBA) were analyzed using XRD patterns, as illustrated in Fig. 1(d). The XRD pattern of pristine P2CBA reveals a broad and prominent peak centered at $2\theta = 22.5°$, which is characteristic of its amorphous nature. This broad peak indicates the presence of a disordered polymeric structure with limited long-range periodicity.

Upon the incorporation of AgCl into the P2CBA matrix, the XRD pattern exhibits additional features indicative of enhanced crystallinity. The modified composite structure shows three weak but distinct peaks at $2\theta = 22.0°$, 30.9°, and 37.8°, which can be attributed to the parallel periodicity of the polymer chains. These newly observed peaks suggest an increase in the ordered regions within the polymer matrix, thereby confirming the development of a semi-crystalline nature in the AgCl–P2CBA complex. The presence of these peaks indicates that the interaction between AgCl and P2CBA induces a partial transformation from an amorphous to a more ordered phase. This structural change could lead to modifications in the optical and electronic properties of the material, making it potentially useful for optoelectronic and catalytic applications.

For AgCl–P2CBA, key diffraction peaks were observed at 67.2°, 56.9°, 54.3°, 45.9°, 32.0°, and 27.4°, corresponding to the crystal planes (400), (222), (311), (220), (200), and (111) of AgCl, respectively. The crystalline structure matches the Joint Committee on Powder Diffraction Standards (JCPDS) file 31-1238.[7,17] Additionally, the XRD analysis revealed three distinct peaks at 38.1°, 30.4°, and 24°, attributed to the P2CBA polymer. Minor peaks corresponding to Ag_2O were also observed. These findings confirm the successful formation of AgCl within the P2CBA polymer matrix. The XRD patterns displayed intense and well-defined diffraction peaks, reflecting the high nanocrystalline nature of the AgCl–P2CBA composite, which enhances its optical properties. The crystallite size was calculated using the Scherrer equation.[18]

$$D = 0.9\lambda/\beta \cos\theta \quad (1)$$

where β is the full width at half maximum (FWHM) in radians, θ is the Bragg's angle, and λ is the X-ray wavelength (CuK$\alpha = 0.154$ nm). The crystallite size of the AgCl–P2CBA composite at the highest peak ($2\theta = 32.0°$) is approximately 40 nm. This relatively small crystallite size, indicative of a high surface area, is particularly advantageous for PEC applications.

3.1.2. SEM morphology. The SEM images of P2CBA and AgCl–P2CBA films, shown in Fig. 2(b) and (c), provide insights into the morphological structure of the fabricated films. The surface morphology of P2CBA, as seen in Fig. 2(a), reveals a non-uniform structure arising from the aggregation of small particles. These particles appear densely packed and intertwined, forming a continuous thin film without any observable holes or cracks. Notably, some particles exhibit elongated, rod-like shapes with length about 0.84 μm. The morphology of the AgCl–P2CBA nanocomposite demonstrates notable alterations compared to pure P2CBA. As shown in Fig. 2(b), the surface of AgCl–P2CBA is characterized by individual particles with irregular shapes and sizes. These particles resemble semispherical nano- and microstones, with sizes ranging from 150 nm to 1.1 μm, separated by wide gaps. This unique structure can enhance the optical properties and facilitate the penetration of electrolytes into the electrode. The 3D topography and surface roughness were analyzed using SEM images processed with the free Gwyddion software. Fig. 2(d) reveals that the P2CBA surface features numerous peaks and valleys with varying depths, heights, and spacing. In comparison, the AgCl–P2CBA surface exhibits a more complex and highly rough morphology, as shown in Fig. 2(d). The larger distances between peaks and valleys indicate a significantly rougher surface with increased surface area.[19] Fig. S1 (SI) shows the particle size distribution of the AgCl–P2CBA nanocomposite. The particles are predominantly in the range of 150–180 nm, indicating a relatively uniform morphology. This narrow size distribution reflects the structural consistency of the nanocomposite, which is essential for achieving stable and reproducible photoelectrochemical performance.

The roughness parameters, such as arithmetic average roughness (R_a) and root mean square roughness (R_q), provide insights into the surface texture irregularities characteristics.[20] P2CBA exhibits an R_a of 133.4 and an R_q of 161.7, while the AgCl–P2CBA displays an R_a of 175.3 and an R_q of 204.7. This enhanced surface roughness suggests that AgCl–P2CBA has a higher surface area with more active sites compared to P2CBA. Additionally, the complex rough morphology is useful for enhancing the interaction between incident photons and the material, increasing light trapping within the material structure and promoting photon absorption.[19] This process generates a large number of electron–hole pairs on the surface of the electrode. This results in improved sensitivity and overall performance of the photodetector.

3.1.3. Optical properties. The light absorption capability of the fabricated AgCl–P2CBA complex nanocomposite is primarily determined by the interaction of its constituent materials with incident photons. When exposed to light, the material absorbs photons and transfers their energy to hot electrons, which are crucial for participating in PEC reactions and hydrogen production. Fig. 3 presents the optical properties of both the pristine P2CBA polymer and the AgCl–P2CBA nanocomposite through absorbance and Tauc spectra.[21,22] The AgCl–P2CBA complex exhibits a broad absorbance spectrum that extends across a wide optical range, including the infrared

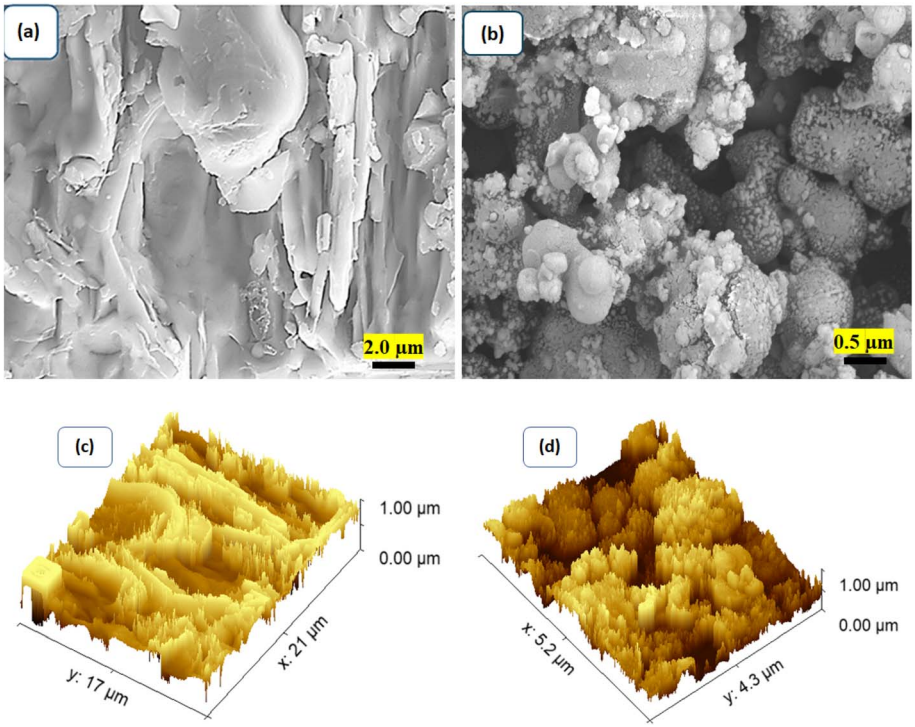

Fig. 2 SEM and 3D roughness of (a and c) P2CBA polymer and (b and d) AgCl–P2CBA nanocomposite.

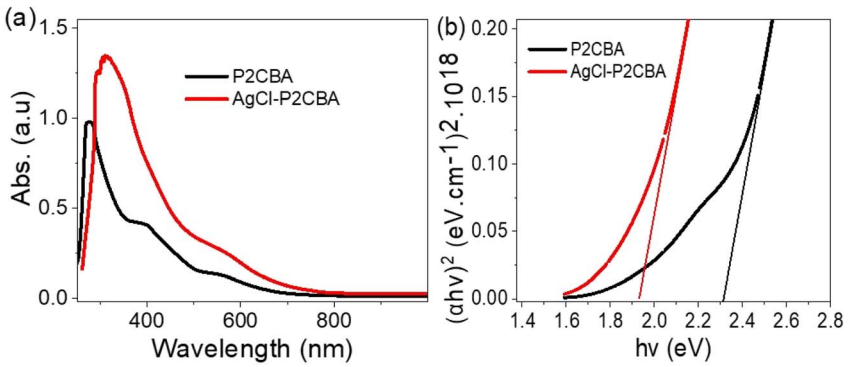

Fig. 3 (a) Optical absorbance (b) Tauc spectra of P2CBA polymer and AgCl–P2CBA nanocomposite.

(IR) region, highlighting its ability to efficiently harness light energy beyond the visible (Vis) spectrum. In contrast, the pristine P2CBA polymer shows a more limited absorption range primarily within the visible region, resulting in lower efficiency in capturing light energy.

The enhanced optical properties of the AgCl–P2CBA complex are attributed to the incorporation of AgCl, which modifies the electronic structure and forms an additional complex network with the polymer. This synergistic effect significantly improves the overall light absorption behavior of the nanocomposite, making it highly suitable for applications such as photocatalysis and solar energy conversion.

To further quantify its optical properties, the absorption coefficient (α) was calculated using the film thickness (d) and material absorbance (A) according to eqn (2). The optical bandgap (E_g) of the AgCl–P2CBA nanocomposite was determined using the Tauc equation, yielding a bandgap energy of 1.92 eV, Fig. 3(b). This low bandgap value confirms the enhanced light-harvesting capabilities of the material, making it a strong candidate for energy-related applications.

$$\alpha = \left(\frac{2.303}{d}\right) A \tag{2}$$

$$\alpha\hbar f = K(hf - E_g)^{1/2} \tag{3}$$

where K is a constant, $\hbar$ is Planck's constant, and f is the photon frequency.

3.2. Application of the H_2 generation

The PEC behavior of P2CBA and AgCl–P2CBA electrodes for hydrogen generation is studied using a three-electrode cell in

a seawater splitting reaction. When light illuminates the electrodes, it excites electrons, generating electron–hole pairs that are fundamental for driving the water-splitting reaction. The amount of hydrogen gas (H_2) produced is directly related to the number of electron–hole pairs generated, which can be estimated by measuring the photocurrent density. Natural seawater, containing heavy metals and salts, acts as an inherent electrolyte, enhancing the electrolysis process without the need for additional synthetic electrolytes.[23,24]

Fig. 4(a) presents the linear sweep voltammetry curves for P2CBA and AgCl–P2CBA electrodes under white light and in the dark. The pristine P2CBA photocathode exhibited a photocurrent density (J_{ph}) of -0.004 mA cm^{-2} and a dark current density (J_o) of -0.018 mA cm^{-2} at -0.95 V *vs.* RHE. In contrast, the AgCl–P2CBA electrode recorded J_{ph} and J_o values of -0.010 mA cm^{-2} and -0.035 mA cm^{-2}, respectively, at the same voltage. This indicates that the photocurrent density of AgCl–P2CBA is twice that of pristine P2CBA, highlighting its enhanced photocatalytic performance. The limited performance of the pristine material suggests a lower efficiency in utilizing incident photons for energy transfer. For the AgCl–P2CBA electrode, the photocurrent density is 3.5 times higher than the dark current. The low dark current of AgCl–P2CBA reflecting the absence of photogenerated electron–hole pairs in the dark. Conversely, the high photocurrent under illumination signifies efficient redox reactions at the electrolyte–electrode interface, underscoring the excellent PEC performance of the AgCl–P2CBA electrode. Additionally, AgCl–P2CBA demonstrates the ability to generate photocurrent without requiring an external voltage, a critical advantage that simplifies PEC systems and reduces energy costs.

The incorporation of AgCl into the P2CBA matrix significantly enhances its light absorption capacity, thereby improving overall photocatalytic activity. This enhancement illustrates the crucial role of AgCl in modifying the electronic structure and facilitating more efficient charge separation, ultimately leading to improved water-splitting efficiency by maximizing light absorption across a broader spectral range. Moreover, the rough morphology of the AgCl–P2CBA structure increases its surface area, creating numerous active sites that enhance the interaction between light, the electrode surface, and the surrounding electrolyte. This improved interaction not only boosts light absorption but also facilitates the redox reactions essential for hydrogen generation. The reduced bandgap and extended light absorption range of AgCl–P2CBA further demonstrate its superior ability to harness a broader spectrum of light, resulting in enhanced electron–hole pair generation. The integration of AgCl with P2CBA improves charge migration to the electrode surface and reduces energy losses during the PEC process. Furthermore, the heterojunction formation between AgCl and P2CBA within the composite minimizes electron–hole recombination by effectively separating charge carriers, ensuring that more electrons and holes participate in the hydrogen evolution reaction (HER). Collectively, these properties contribute to a higher photocurrent density and improved PEC performance, highlighting the feasibility of using seawater as a renewable and abundant resource for hydrogen production through solar energy conversion, thereby addressing global energy challenges while supporting green energy initiatives.

The stability test is an essential evaluation of the performance and durability of photoelectrodes, particularly in PEC applications. For the AgCl–P2CBA photoelectrode, stability was assessed using the chopped current method under alternating light (on/off) conditions, as depicted in Fig. 4(b). Upon illumination, the photocathode absorbs light, generating electron–hole pairs and leading to an increase in current density, while in darkness, the current density decreases. The sequential fluctuations in current density reflect the photoelectrode's rapid response to light stimuli. Consistent variations across multiple cycles underscore the sensitivity and reproducibility of the AgCl–P2CBA photoelectrode, confirming its stable performance even after repeated light exposure. The photoelectrode's high sensitivity demonstrates its ability to efficiently capture light energy and convert it into photocurrent, a key process for hydrogen generation. AgCl–P2CBA's durability indicate strong the chemical and structural stability of AgCl–P2CBA. Additionally, its anticorrosion properties enhance its resilience, enabling it to withstand degradation and maintain functionality in harsh environments, such as seawater with salts and heavy metals. Stability is further supported by the photoelectrode's efficient electron transfer at the electrode–electrolyte interface. The heterojunction between AgCl and P2CBA

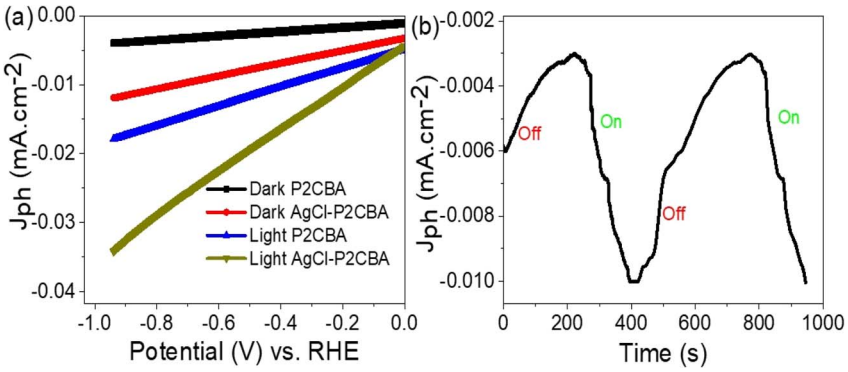

Fig. 4 (a) The PEC response of the fabricated P2CBA and AgCl–P2CBA for H_2 gas generation from splitting Red Sea water under white light (b) on/off chopped light for AgCl–P2CBA composite electrode.

effectively reduces electron–hole recombination. These findings underscore the exceptional reliability and effectiveness of AgCl–P2CBA for practical PEC water-splitting and hydrogen evolution reactions (HER).

The Tafel plot in Fig. S2 illustrates the PEC behavior of the AgCl–P2CBA nanocomposite under illumination at various wavelengths (340, 440, 540, and 730 nm). It shows the relationship between the applied potential (*vs.* RHE) and the logarithm of the photocurrent density ($\log J_{ph}$), highlighting the strong dependence of PEC performance on the incident light wavelength. At shorter wavelengths (340 and 440 nm), the nanocomposite demonstrates lower overpotentials for hydrogen evolution, indicating more favorable kinetics. For instance, at a fixed $\log J_{ph}$ value of 6.0, the overpotential for 340 nm illumination is significantly lower compared to that at longer wavelengths. This behavior underscores the enhanced generation and separation of charge carriers driven by higher-energy photons, which effectively excite electrons across the bandgap of the AgCl–P2CBA material and accelerate the HER. In contrast, as the illumination shifts to longer wavelengths (540 and 730 nm), a noticeable increase in overpotential is observed. This trend reflects diminished light absorption and weaker charge carrier excitation due to the lower photon energy, especially near the infrared region. Consequently, the reduced efficiency in charge separation and transport hinders the HER, requiring a higher energy input to sustain similar photocurrent densities. These findings confirm that the PEC activity of AgCl–P2CBA is highly wavelength-dependent, with optimal performance under higher-energy illumination. Therefore, AgCl–P2CBA emerges as a promising candidate for PEC hydrogen generation, particularly under solar light conditions where shorter wavelengths are present.

Photon energies are vital for exciting electron levels within the photoelectrode, facilitating the generation of photocarriers. The photo-response of the AgCl–P2CBA photoelectrode was examined under illumination with light of different wavelengths, using natural seawater as the electrolyte, as shown in Fig. 5(a). Optical filters were employed to control the photon wavelengths at 340, 440, 540, and 738 nm, corresponding to photon energies of 3.64, 2.81, 2.29, and 1.68 eV, respectively. The J_{ph} was measured under an applied bias voltage of −0.95 V shown in Fig. 5(b). At longer wavelengths (738 nm), the photocathode displayed minimal responsivity, with a low J_{ph} of approximately −0.020 mA cm^{-2}. In contrast, at shorter wavelengths (340 nm), the photocathode exhibited significantly higher responsivity, with J_{ph} reaching −0.035 mA cm^{-2}. This variation in responsivity underscores the AgCl–P2CBA photoelectrode's ability to efficiently absorb and utilize photon energy at shorter wavelengths. Photons with lower energies are unable to induce the necessary electron transitions, leading to reduced efficiency. Higher-energy photons (shorter wavelengths) promote increased electron–hole pair generation.[25] These photogenerated carriers contribute to the formation of OH radicals, which play a crucial role in the production of H_2 from water, enhancing PEC performance.

The amount of H_2 gas evolution from the AgCl–P2CBA photoelectrode is illustrated in Fig. 6(a). The production rate of H_2 gas is estimated to be 3.5 μmol h^{-1} for a 1 cm^2 area. This significant value highlights the efficacy of the photocathode, especially given its fabrication through a single-step process suitable for mass production. Furthermore, its cost-effectiveness enhances its potential as a viable solution for renewable energy production, particularly in generating H_2 gas from seawater.

To elucidate the enhanced PEC performance of the AgCl–P2CBA nanocomposite, a charge transfer mechanism based on energy band alignment is proposed and illustrated in Fig. 6(b). The improved hydrogen evolution is primarily attributed to the formation of a heterojunction between AgCl and the conducting polymer P2CBA, which facilitates efficient charge separation and directional charge transfer.[26–28] The combination of AgCl's wide bandgap and P2CBA's narrower bandgap creates favorable energy offsets that promote interfacial charge movement. Upon light irradiation, both materials generate electron–hole pairs. Electrons in AgCl's conduction band migrate to the lower-lying LUMO of P2CBA and subsequently to the electrolyte interface (natural Red Sea water), where they reduce protons to form hydrogen gas.[29,30] Simultaneously, holes in P2CBA's HOMO transfer to AgCl's valence band, minimizing recombination. The ion-rich seawater further enhances charge mobility and supports hydrogen evolution at the electrode–electrolyte interface. This directional flow of charge carriers and the optimized

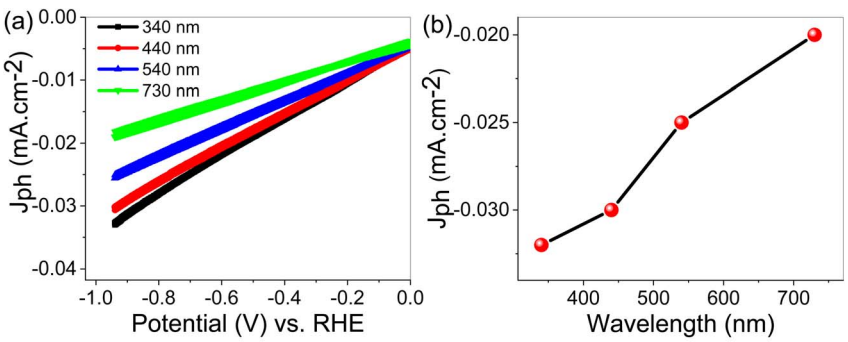

Fig. 5 (a) The PEC response of the AgCl–P2CBA under light with various wavelengths (b) the evaluated J_{ph} for photons with different wavelengths.

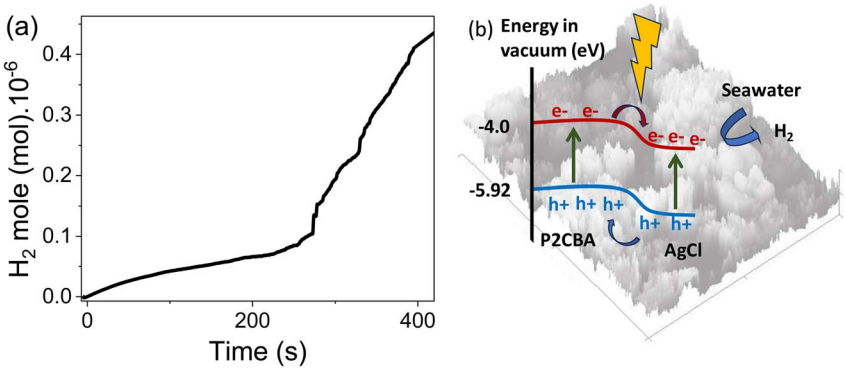

Fig. 6 (a) Evaluation of the estimated hydrogen moles (b) schematic diagram of the charge transfer through the constituents of for the AgCl–P2CBA photoelectrode.

Table 2 Comparison of the electrochemical performance of the AgCl–P2CBA photocathode with other reported photocathodes

Photoelectrode	J_{ph} (mA cm^{-2})	Electrolyte
Cr_2S_3–Cr_2O_3/ poly-2-aminobenzene-1-thiol[23]	0.017	Sewage water
g-C_3N_4–CuO [31]	0.01	NaOH
CuO–C/TiO_2 [32]	0.012	Glycerol
TiN–TiO_2 [33]	3.0×10^{-4}	NaOH
Present work: AgCl–P2CBA	0.035	Red sea water

band alignment ensure efficient separation and utilization of photogenerated charges. Overall, these results highlight the strong potential of AgCl–P2CBA as a light-responsive photocathode for efficient seawater-splitting applications.

Finally, Table 2 presents a comparative overview of the electrochemical performance of the AgCl–P2CBA photocathode relative to various previously reported systems. The results clearly demonstrate its superior PEC activity, underscoring the effectiveness of the AgCl–P2CBA nanocomposite for efficient hydrogen generation.

4. Conclusion

A novel AgCl–P2CBA photocathode has been successfully developed through a cost-effective and efficient one-step fabrication method. This advanced material is designed for sustainable energy applications, with a primary focus on hydrogen production from seawater. XRD analysis revealed a crystallite size of approximately 40 nm, while FTIR spectroscopy showed characteristic shifts in functional group positions following AgCl incorporation, confirming successful composite formation. The PEC performance of both pristine P2CBA and AgCl–P2CBA photocathodes was evaluated for hydrogen evolution. The AgCl–P2CBA composite demonstrated a markedly enhanced photocurrent density of −0.035 mA cm^{-2}, nearly twice that of pristine P2CBA. Furthermore, it achieved a hydrogen production rate of 3.5 μmol h^{-1} cm^{-2}. This performance enhancement is attributed to improved charge separation and transfer, along with increased light absorption, underscoring the beneficial role of AgCl in enhancing photocatalytic activity. Beyond its PEC efficiency, the AgCl–P2CBA nanocomposite offers notable economic advantages. Its low-cost synthesis and scalability *via* a simple one-pot method make it a strong candidate for industrial-scale hydrogen production. Given its high efficiency, affordability, and ease of fabrication, the AgCl–P2CBA photocathode represents a promising solution for next-generation hydrogen technologies. Its integration into future hydrogen-based energy infrastructures could significantly contribute to global decarbonization efforts and the transition to clean energy.

Ethical statement

This study does not include any humans or animal studies.

Conflicts of interest

The authors have no conflict of interest.

Data availability

All data generated or analyzed during this study are included in this article.

Supplementary information: figures of particle distribution and Tafel plot for the synthesized AgCl-P2CBA nanocomposite. See DOI: **https://doi.org/10.1039/d5ra03341a**.

Acknowledgements

This research has been funded by Scientific Research Deanship at University of Ha'il – Saudi Arabia through project number ≪RG-24 062≫.

References

1 E. Aldosari, M. Rabia, Q. Zhang and S. H. Mohamed, High-efficiency photocathode for green hydrogen generation from sanitation water using bismuthyl chloride/poly-*o*-chlorobenzeneamine nanocomposite, *Open Chem.*, 2025, **23**, 20240112.

2 R. Keshavarzi, M. Mousavian, M. K. Omrani, V. Mirkhani, N. Afzali, C. A. Mesa, I. Mohammadpoor-Baltork and S. Gimenez, Photoelectrochemical water splitting with dual-photoelectrode tandem and parallel configurations: enhancing light harvesting and carrier collection efficiencies, *Surf. Interfaces*, 2023, **38**, 102813.

3 A. A. Mohd Raub, R. Bahru, S. N. A. Mohd Nashruddin and J. Yunas, Advances of nanostructured metal oxide as photoanode in photoelectrochemical (PEC) water splitting application, *Heliyon*, 2024, **10**.

4 E. Aldosari, M. Rabia, A. Sanna and O. Farid, Single-step fabrication of Ag_2S/poly-2-mercaptoaniline nanoribbon photocathodes for green hydrogen generation from artificial and natural red-sea water, *Open Phys.*, 2025, **23**, 20240095.

5 S. Uemura, R. Kobayashi, S. Ikegami, Y. Aoyama and Y. Tabe, Electricity storage and hydrogen generation system using the electrochemical reaction of lithium and water, *Int. J. Hydrog. Energy*, 2025, **100**, 853–862.

6 Y. Y. Dong, Y. H. Zhu, M. G. Ma, Q. Liu and W. Q. He, Synthesis and characterization of Ag@AgCl-reinforced cellulose composites with enhanced antibacterial and photocatalytic degradation properties, *Sci. Rep.*, 2021, **11**, 1–9.

7 D. Li, L. Ouyang, L. Yao, L. Zhu, X. Jiang and H. Tang, *In Situ* SERS Monitoring the Visible Light Photocatalytic Degradation of Nile Blue on Ag@AgCl Single Hollow Cube as a Microreactor, *ChemistrySelect*, 2018, **3**, 428–435.

8 A. Jakimińska and W. Macyk, Photochemical transformations of AgCl in the context of its eventual photocatalytic applications, *J. Photochem. Photobiol., A*, 2023, **445**, 115048.

9 E. Aldosari, M. Rabia and A. A. A. Abdelazeez, Rod-shaped Mo(VI) trichalcogenide-Mo(VI) oxide decorated on poly(1-*H* pyrrole) as a promising nanocomposite photoelectrode for green hydrogen generation from sewage water with high efficiency, *Green Process. Synth.*, 2024, **13**, 20230243.

10 J. Yan, L. Hu, L. Cui, Q. Shen, X. Liu, H. Jia and J. Xue, Synthesis of disorder-order TaON homojunction for photocatalytic hydrogen generation under visible light, *J. Mater. Sci.*, 2021, **56**, 9791–9806.

11 A. Singh and A. Chandra, Graphite oxide/polypyrrole composite electrodes for achieving high energy density supercapacitors, *J. Appl. Electrochem.*, 2013, **43**, 773–782.

12 H. M. El-Bery, M. M. Abdel Naby, G. G. Mohamed, M. E. El-Khouly and M. B. Zakaria, Enhancing photocatalytic hydrogen generation on TiO_2 using thermally derived nickel-based cocatalysts from Hofmann-type cyanide coordination polymer flakes, *Int. J. Hydrogen Energy*, 2024, **78**, 470–480.

13 M. Rabia, A. Ben Gouider Trabelsi, F. H. Alkallas and A. M. Elsayed, One pot synthesizing of cobalt(III) and (IV) oxides/polypyrrole nanocomposite for light sensing in wide optical range, *Phys. Scr.*, 2024, **99**, 035523.

14 F. H. Alkallas, A. M. Elsayed, A. B. G. Trabelsi and M. Rabia, Porous-spherical MnO_2-$Mn(OH)_2$/polypyrrole nanocomposite thin film photodetector in a wide optical range from UV to IR, *Opt. Quantum Electron.*, 2023, **55**, 1–15.

15 E. M. S. Azzam, H. M. Abd El-Salam and R. S. Aboad, Kinetic preparation and antibacterial activity of nanocrystalline poly(2-aminothiophenol), *Polym. Bull.*, 2019, **76**, 1929–1947.

16 S. A. Hameed, H. A. Ewais and M. Rabia, Dumbbell-like shape Fe_2O_3/poly-2-aminothiophenol nanocomposite for two-symmetric electrode supercapacitor application, *J. Mater. Sci.: Mater. Electron.*, 2023, **34**, 1–8.

17 J. Wang, C. An, M. Zhang, C. Qin, X. Ming and Q. Zhang, Photochemical conversion of AgCl nanocubes to hybrid AgCl-Ag nanoparticles with high activity and long-term stability towards photocatalytic degradation of organic dyes, *Can. J. Chem.*, 2012, **90**, 858–864.

18 A. M. Ahmed, M. Rabia and M. Shaban, The structure and photoelectrochemical activity of Cr-doped PbS thin films grown by chemical bath deposition, *RSC Adv.*, 2020, **10**, 14458–14470.

19 A. M. Salem, A. R. Mohamed, A. M. Abdelghany and A. Y. Yassin, Effect of polypyrrole on structural, optical and thermal properties of CMC-based blends for optoelectronic applications, *Opt. Mater.*, 2022, **134**, 113128.

20 R. Saad, K. Abdelkarem, A. M. Ahmed, M. Zayed, Z. M. Faidey, M. Shaban, M. T. Tammam and H. Hamdy, Enhanced CO_2 gas sensing at room temperature using Ag-plated Na-doped CuO thin films synthesized by successive ionic layer adsorption and reaction technique, *Surf. Interfaces*, 2024, **44**, 103789.

21 K. Baishya, J. S. Ray, P. Dutta, P. P. Das and S. K. Das, Graphene-mediated band gap engineering of WO_3 nanoparticle and a relook at Tauc equation for band gap evaluation, *Appl. Phys. A: Mater. Sci. Process.*, 2018, **124**, 1–6.

22 Ł. Haryński, A. Olejnik, K. Grochowska and K. Siuzdak, A facile method for Tauc exponent and corresponding electronic transitions determination in semiconductors directly from UV-Vis spectroscopy data, *Opt. Mater.*, 2022, **127**, 112205.

23 H. Xie, Z. Zhao, T. Liu, Y. Wu, C. Lan, W. Jiang, L. Zhu, Y. Wang, D. Yang and Z. Shao, A membrane-based seawater electrolyser for hydrogen generation, *Nature*, 2022, **612**, 7941.

24 S. Moradi-Alavian, A. Kazempour, M. Mirzaei-Saatlo, H. Ashassi-Sorkhabi, A. Mehrdad, E. Asghari, J. J. Lamb and B. G. Pollet, Promotion of hydrogen evolution from seawater *via* poly(aniline-*co*-4-nitroaniline) combined with 3D nickel nanoparticles, *Sci. Rep.*, 2023, **13**, 1–10.

25 F. H. Alkallas, A. B. G. Trabelsi, T. A. Alrebdi and M. Rabia, Fabrication of WO_2I_2/poly *o*-amino thiophenol porous spherical-nanocomposite with promising optical absorbance for photodetector device applications, *Opt. Quantum Electron.*, 2025, **57**(150), 1–16.

26 J. Xue, H. Zhang, Q. Shen, W. Zhang, J. Gao, Q. Li, X. Liu and H. Jia, Enhanced photoelectrocatalytic hydrogen production

performance of porous MoS_2/PPy/ZnO film under visible light irradiation, *Int. J. Hydrogen Energy*, 2021, **46**, 35219–35229.

27 X. Li, W. Wang, F. Dong, Z. Zhang, L. Han, X. Luo, J. Huang, Z. Feng, Z. Chen, G. Jia and T. Zhang, Recent Advances in Noncontact External-Field-Assisted Photocatalysis: From Fundamentals to Applications, *ACS Catal.*, 2021, **11**, 4739–4769.

28 G. Konstantatos, M. Badioli, L. Gaudreau, J. Osmond, M. Bernechea, F. Pelayo, G. De Arquer, F. Gatti and F. H. L. Koppens, Hybrid graphene-quantum dot phototransistors with ultrahigh gain, *Nat. Nanotechnol.*, 2012, **7**, 363.

29 M. Rabia, A. B. G. Trabelsi, A. M. Elsayed and F. H. Alkallas, Porous-Spherical Cr_2O_3-$Cr(OH)_3$-Polypyrrole/Polypyrrole Nanocomposite Thin-Film Photodetector and Solar Cell Applications, *Coatings*, 2023, **13**(7), 1240.

30 X. Tian, Y. Chen, Y. Chen, D. Chen, Q. Wang and X. Li, Removal of Gaseous Hydrogen Sulfide by a $FeOCl/H_2O_2$ Wet Oxidation System, *ACS Omega*, 2022, **7**, 8163–8173.

31 V. Ragupathi and M. A. Raja, CuO/g-C_3N_4 nanocomposite as promising photocatalyst for photoelectrochemical water splitting, *Optik*, 2020, **208**, 164569.

32 X. Huang, M. Zhang and R. Sun, Enhanced hydrogen evolution from CuOx-C/TiO_2 with multiple electron transport pathways, *PLoS One*, 2019, **14**, 0215339.

33 A. Naldoni, U. Guler and Z. Wang, Broadband hot-electron collection for solar water splitting with plasmonic titanium nitride, *Adv. Opt. Mater.*, 2017, **5**, 1601031.